Journal of Electroanalytical Chemistry 887 (2021) 115169

Contents lists available at ScienceDirect

Journal of Electroanalytical Chemistry

journal homepage: www.elsevier.com/locate/jelechem

In situ potentiometric SECM monitoring of the extracellular pH changes under electrical stimulation using a dual-microelectrode tip

Qiang Xiong, Ranran Song, Tao Wu, Fan Zhang *, Pingang He *

School of Chemistry and Molecular Engineering, East China Normal University, 500 Dongchuan Road, Shanghai 200241, PR China

ARTICLE INFO

Keywords:
Scanning electrochemical microscopy (SECM)
Extracellular pH
pH-selective dual-microelectrode tip
Electrical stimulation

ABSTRACT

Different cells respond differently to environmental stimulation, resulting in different extracellular pH values. Therefore, the pH of the extracellular microenvironment (pHe) is an important manifestation of cell response to the environment. In this study, a pH-selective dual-microelectrode tip was used as the probe tip of a scanning electrochemical microscopy (SECM) instrument to in situ monitor the pHe changes of different cells after being electrically stimulated by the SECM potential method. pHe is the pH at a certain distance from the cells, and the distance is determined by substituting the current measured by the approach curve into a theoretical calculation. A gold microelectrode was used to determine the distance between the dual-microelectrode tip and the cell, and a pH-selective microelectrode was used to measure the pHe. It was found that the pHe value was related to the distance between the pH-measuring electrode and the cell, and different types of cells had different pHe changes after electrical stimulation. Through fluorescent staining with calcein-AM and propidium iodide, it was verified that this phenomenon was caused by changes in the permeability of the cell membrane due to electrical stimulation. In situ monitoring the pHe changes of different cells will be helpful for exploring the response of cells to environmental stimulation and the mechanism of these different responses.

1. Introduction

Cells are the basic structural and functional units of organisms and the main sites of metabolism [1]. The acidification of the extracellular microenvironment can mark the progression of cancer [2,3]. Its minor changes will affect the activity of many biological proteases, which in turn affect various life processes, such as ion transport, nucleic acid formation and metabolite release [4,5]. Thus, an acid-base balance plays a vital role in maintaining physiology and cell response, and extracellular pH (pHe, refers to the pH of the extracellular microenvironment) is one of the important regulatory factors in physiological activities of cells [6]. Deviations from normal pHe values can damage the cellular immune response, such as inhibiting the activity of lymphocytes [7]. On the other hand, when cells are stimulated, the extracellular microenvironment will change, and the pHe will also change accordingly. For example, infrared light can change the distribution of ions on the cell membrane surface and cause changes in membrane capacitance [8]; additionally, cell membrane permeability changes with the stimulation of heavy metals [9,10]. It can be seen that the change in pHe is an important manifestation of the cell response to the environment [5]. Therefore, an accurate observation of cell pHe changes in situ is very important to understand the mutation process of cells under the influence of the environment [11,12].

To date, the methods for measuring pHe are the fluorescence [13–16] and surface enhanced Raman techniques [5,17–19]. For fluorescence detection, a pH fluorescence probe is usually required to modify the cell surface [16]. However, the photobleaching and quenching of fluorescent probes may have a long-term effect on the detection of pH, thereby affecting its accuracy [20]. The surface-enhanced Raman technique also requires the introduction of probe molecules to detect pHe, which may also change the physiological state of cells [1]. In addition, technologies, such as ion-sensitive field effect transistors [21] and magnetic resonance imaging [22,23], are also used to detect pHe. However, the spatial resolution of these methods is low, and they rely on the distribution of probes in the tissue, which makes the quantification of pHe observed in situ challenging. Scanning electrochemical microscopy (SECM) is a powerful scanning probe technology. It has a wide range of applications in evaluation of living cells. Arūnas Ramanavičius's group had carried out SECM research on active and inactive cells [24], and investigation of mammalian (human) cell activity [25,26]. They have also reported the application of various redox mediators in SECM imaging of yeast cells,

* Corresponding authors at: School of Chemistry and Molecular Engineering, East China Normal University, 500 Dongchuan Road, Shanghai 200241, PR China.
E-mail addresses: fzhang@chem.ecnu.edu.cn (F. Zhang), pghe@chem.ecnu.edu.cn (P. He).

https://doi.org/10.1016/j.jelechem.2021.115169
Received 16 November 2020; Received in revised form 10 March 2021; Accepted 15 March 2021
Available online 24 March 2021

and evaluated the influence of pH on their bioelectrochemical activity [27,28]. Dipankar Koley's group successfully used pH-selective microelectrodes (hydrogen-ion carriers and polyaniline films) as scanning electrochemical microscopy probes to image the pH distribution of bioactive glass and bacterial biofilms [29]. Munteanu et al. designed a voltammetric pH microsensor to monitor the pHe of mammalian cells at different oxygen levels [30]. Our group reported a technique of in situ observation of pHe using a dual-microelectrode tip for pH-potentiometric sensing with SECM [31]. Moreover, the combination of scanning electrochemical microscopy and other technologies, such as fast Fourier transform - scanning electrochemical impedance microscopy (FFT-SEIM), provides new possibilities in fast gathering of informative electrochemical signal [32–34].

Here, the dual-microelectrode tip was further used for pH potential sensing with SECM to observe the pHe changes of different cells under electrical stimulation in situ. Compared with our previous work [31], the distance between the tip of the microelectrode and cell surface was more accurately described using the negative feedback theory, thus increasing the determination accuracy of the pHe microenvironment. Moreover, it was found that normal cells and cancer cells respond differently to electrical stimulation. By in situ observation, it was shown that the pHe of cancer cells was lower than that of normal cells in the absence of stimulation. At low potential stimulation, the pHe of cancer cells did not change significantly, but with the increase in stimulation potential, the pHe changed significantly. In regard to normal cells, the pHe showed significant changes at low potential stimulation, while at higher potential stimulation, the pHe of normal cells showed little change. This phenomenon probably reveals the changes in the membrane permeability of cancer cells and normal cells after stimulation, which has potential value for further research on the response of different cells to different environmental stimuli.

2. Experimental section

2.1. Chemicals and materials

Ferrocene methanol (FcMeOH) was purchased from Sigma-Aldrich (USA). Aniline was obtained from Sinopharm Chemical Reagent Co., LTD. Dulbecco's modified Eagle's medium (DMEM), trypsin/EDTA solution, penicillin/streptomycin (P/S), nonessential amino acids, glutamine, sodium pyruvate solution and fetal bovine serum (FBS) solution were obtained from Thermo Fisher (Waltham, MA, USA). Calcein-AM/propidium iodide suitable for fluorescence was obtained from Dojindo Chemical Technology Co., Ltd. (Shanghai, China). ITO (indium tin oxide, 4 cm × 5 cm, sheet resistance < 7 Ω/sq) glass was provided by Zhuhai Kaivo Optoelectronic Technology Co., Ltd. (China). Borosilicate glass capillary (1.0 mm OD × 0.75 mm ID) tubing was obtained from Sutter Instrument Company (USA). Gold (d = 25 μm) and platinum wires (d = 25 μm) were purchased from Alfa Aesar (USA). Phosphate-buffered saline (PBS, 0.01 M, pH = 7.40) was prepared with deionized water (DI, 18.2 MΩ·cm). The human breast cancer cell line (MCF-7), human cervical cancer cell line (HeLa) and human foreskin fibroblasts (HFFs) were obtained from the Chinese Academy of Sciences (Shanghai, China).

2.2. Instruments

MCF-7, HFF, and HeLa cells were cultured in a humidified incubator (NuAire, USA). The pH detection was carried out using a CHI 920C scanning electrochemical microscope (CH Instruments Co., Shanghai, China). MCF-7, HFF and HeLa cells were electrically stimulated using a CHI 830B electrochemical workstation (CH Instruments Co., Shanghai, China) with a HEKA ELP-3 system (HEKA, Germany). Drawing borosilicate glass capillary tubes was performed on a P-2000 laser puller (Sutter Instrument Company, USA).

2.3. Preparation of the dual-microelectrode tip

The dual-microelectrode tip used in SECM for the combined amperometric/potentiometric operation was prepared according to a previously reported method [31]. Briefly, a borosilicate glass tube with an inner diameter of 0.75 mm was drawn with a laser puller. By grinding the drawn glass tube with sandpaper, a capillary tube with an inner diameter of 60 ~ 100 μm was obtained. Platinum and gold wires coated with polyimide were inserted into the capillary tube. A certain amount of epoxy resin was injected for encapsulation, and then the capillary tube was dried and polished to obtain a dual-microelectrode tip: a gold microelectrode with a diameter of 25 μm and a platinum microelectrode with a diameter of 25 μm. The platinum microelectrode was modified with polyaniline by cyclic voltammetry to obtain a pH-selective microelectrode. Prior to the electropolymerization of aniline, the platinum microelectrode was electrochemically cleaned in 0.5 M H_2SO_4 by cyclic voltammetry in a potential range of −0.25 to 1.55 V. The polyaniline film was obtained from 0.1 M aniline solution containing 1 M HCl in a potential range of −0.1 ~ 0.9 V at a scanning speed of 10 mV/s over 15 cycles. Polymerization in HCl supporting electrolyte generated smooth morphology of polyaniline. The pH-selective microelectrode was calibrated in a series of standard solution with biologically relevant pH values before the extracellular pH was measured versus the Ag/AgCl reference electrode.

2.4. Cell culture and seeding onto the ITO substrate

MCF-7 and HeLa cells were cultured in DMEM supplemented with 10% FBS and 100 μg/mL P/S at 37 °C in a humidified atmosphere containing 5% CO_2. HFF cells were cultured in DMEM supplemented with 10% FBS, 100 μg/mL P/S and nonessential amino acids, glutamine and sodium pyruvate at 37 °C in a humidified atmosphere containing 5% CO_2. When reaching 80% confluence, the cells were detached with 0.25% trypsin/EDTA. After trypsin was removed, the cells were resuspended in the culture medium. The cells were stained and counted using trypan blue solution. Finally, cells with a specific density were planted on a 0.28 cm^2 ITO substrate for further investigation.

2.5. Determination of the distance between the dual-microelectrode tip and cells

First, the approach curve of the Au microelectrode over the cells was determined at + 0.450 V (vs Ag/AgCl) in 0.01 M PBS solution containing 1.0 mM FcMeOH. The dual-microelectrode tip was moved over the cell at a scan rate of 0.5 μm/s, and when the current of the Au microelectrode decreased to a certain proportion of the limiting steady diffusion current, the tip stopped moving. Substituting the radius of the microelectrode, the ratio of the radius of the insulating sheath to the radius of the electrode tip, and the ratio of the tip current to the limiting steady diffusion current into Formula 2 could obtain the distance between the dual-microelectrode tip and cells.

2.6. In situ monitoring of the extracellular pH under electrical stimulation

After the dual-microelectrode tip approached a certain position, 0.01 M PBS containing 1 mM FcMeOH was replaced by 0.01 M PBS (pH = 7.40). Then, MCF-7, HFF and HeLa cells were stimulated when different constant potentials were applied for 60 s with a three-electrode system. The ITO substrate, Ag/AgCl electrode and Pt wire were used as the working, reference and counter electrodes, respectively. The pH-selective microelectrode was used to measure the potential at this position, and then the microelectrode was lifted to measure the potential in the bulk solution. According to Formula 1, the pHe was calculated by the change in potential divided by the pH response slope of the microelectrode.

3. Results and discussion

3.1. Characterization and response characteristics of the pH-selective microelectrode

The SEM image of the dual-microelectrode tip surface in Fig. 1A clearly displays both microelectrodes with diameters of 25.0 μm, and also a uniform polyaniline layer on the surface of the pH-selective microelectrode (bottom) with the thickness in sub-micron level. The size of the microelectrodes was further characterized by cyclic voltammetry (CV), As shown in Figure S1, the response curves of Au and platinum microelectrodes both display a sigmoidal shape. The radius of microelectrode was then calculated by the equation of $I_{ss} = 4nFDCr_{eff}$. By substituting the values into the equation ($3.9 \times 10^{-9} = 4 \times 1 \times 96485 \times 7.8 \times 10^{-10} \times 1 \times r_{eff}$), the radius is calculated as 12.96 μm, which is consistent with the SEM characterization.

The CV curve recorded in the process of aniline electropolymerization is exhibited in Figure S2. The peak at 0.25 V corresponds to the formation of radical cations, and the peak at 0.85 V is likely caused by the conversion from an emeraldine to a pernigraniline structure, which indicates regular growth of the polymer film. Two reduction peaks at 0.55 V and 0.1 V appear due to the conversion from pernigraniline to emeraldine and from emeraldine to leucoemeraldine, respectively [31]. At the beginning of the electropolymerization, no peaks are presented. As this process proceeds, the peak current is gradually enhanced, indicating that the film formed by electropolymerization is more and more conductive and electroactive. Because these redox peaks are typical CV responses of polyaniline produced by electropolymerization, indicating that the polyaniline film has been successfully modified on the platinum microelectrode [35].

The potentiometric response of the pH-selective microelectrode in the dual-microelectrode tip was further determined in standard buffer solution. From Fig. 1B, it could be observed that the microelectrode shows a linear correlation between the potential and pH value in a range of 4–8. The determination with six randomly selected pH-selective microelectrodes (Table 1) reveals a response slope of -53.2 ± 0.3 mV/pH ($R^2 = 0.999$), displaying Nernstian behavior. The relative standard deviation of 0.64% indicates an excellent reproducibility of the pH-selective microelectrode. In addition, when pH changed from 7.30 to 6.40, 90% of the steady-state signal was yielded in less than 5 s, and a completely stable response was obtained within 20 s. Therefore, the response time [36] could be determined as 10 s. Compared with other literatures [29,30], the pH-selective microelectrode shows good performance, and the response range also could meet the needs of cell detection.

Since each pH-selective microelectrode might have different initial potentials, the pH values could be calculated according to Formula 1.

$$pH = pH_0 - \Delta E/S \quad (1)$$

where pH_0 is the pH value of the bulk solution detected by the pH meter, ΔE is the difference between the open-circuit potential value detected at any position in the solution and that of bulk solution, and S is the response slope.

3.2. Determination of the distance between the dual-microelectrode tip and the cell

In general, pHe refers to the pH at a certain distance very close to the cell. Although there was a good correlation between the normalized current value and the distance from the electrode to the cell surface [33], we still hope to express it directly in terms of distance.

According to the theoretical formula for the negative feedback of SECM [37], there is a functional relationship between the normalized current and distance. In Formula 2, the normalized negative feedback current is the ratio of the tip current to the limiting steady diffusion current. The distance (d) between the tip and the cell can be obtained from the normalized negative feedback current (I_T).

$$I_T = \frac{\frac{2.08}{R_G^{0.358}}\left(\frac{d}{a} - \frac{0.145}{R_G}\right) + 1.585}{\frac{2.08}{R_G^{0.358}}\left(\frac{d}{a} + 0.0023R_G\right) + 1.57 + \frac{\ln R_G}{\frac{d}{a}} + \frac{2}{\pi R_G}\ln\left(1 + \frac{\pi R_G}{2\frac{d}{a}}\right)} \quad (2)$$

where d is the distance between the tip and cell, a is the radius of the microelectrode, r_g is the radius of the insulating sheath, and RG equals r_g/a. When a and r_g are known, the functional relationship between d and I_T can be derived. In other words, according to the normalized current value, the distance between the tip and cell can be calculated.

To verify the validity of Formula 2 more accurately, the tip with 5 μm in the radius of the microelectrode and 25 μm in r_g was

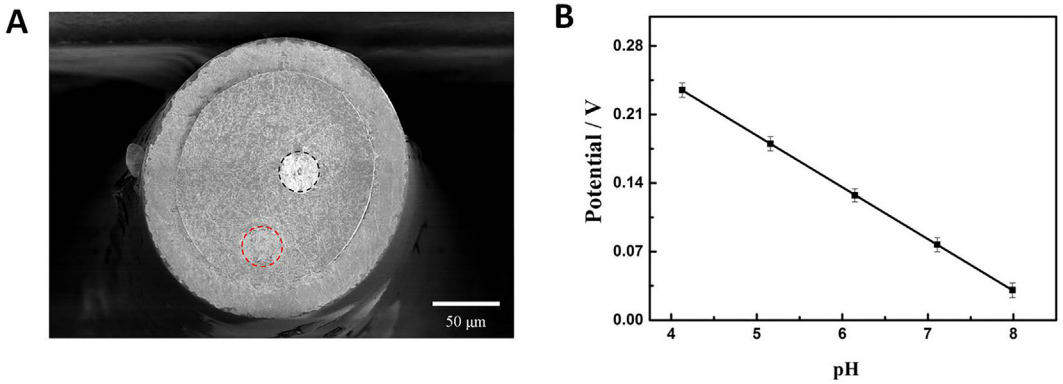

Fig. 1. (A) SEM images of the dual-microelectrode tip, consisting of. Au microelectrode (black dotted line) and polyaniline-modified Pt microelectrode (red dotted line). (B) Linear relationship between the potential of the pH microelectrode and pH values in a range of 4–8.

Table 1
Reproducibility of the pH-selective microelectrode.

Slope (mV/pH)						Average slope (mV/pH)	RSD
1	2	3	4	5	6	53.2	0.64%
53.3	52.9	53.4	53.5	52.6	53.2		

employed, thus obtaining an approach curve by theoretical simulation (Figure S3) and the theoretical curve of the functional relationship between the normalized negative feedback current (I_T) and the tip-cell distance (d) (Fig. 2). The theoretical distance could be verified by the SECM shear force method [38–40]. The vibration frequency of the tip in the solution and on the cell was first determined. As shown in Figure S4, the smaller value obtained on the cell than that in the solution (marked by the arrow in the figure) was selected for the determination. For example, the negative feedback normalized current was set as 0.75, and when the tip approached 0.75, the shear force mode was used to drop the tip until the vibration frequency changed. Then, the tip stopped, and the distance that the tip moved was the distance between the tip and cell. Although the cell surface is not flat, the size of the dual-microelectrode tip was larger than the cell, and it can completely cover the cell. To measure the distance from the electrode to the cell, the electrode was positioned over the cell and the uneven cell surface should have little effect on the calculation of the distance. In addition, FcMeOH, as the redox mediator, is cell membrane permeable, and it has a certain effect on the tip current and then the determination of tip-cell distance. However, this effect would be significant only when the tip was very close to the cell, and it would be negligible when the tip was far away from the cell, thus showing almost no influence on the determination results [10].

Corresponding to different normalized currents, the distances were experimentally measured (Table 2). Fig. 2 indicates that the experimental values were basically consistent with the theoretical curve, and thus the actual distance between the tip and the cell could be obtained by determining the normalized current value. It means that when the current of the dual-microelectrode tip decreases to a certain proportion of the limiting steady diffusion current, the dual-microelectrode tip is located at a precise distance over the cell.

3.3. pHe values of three cell types

The pHe values of three cell types were further investigated at different distances from the cells. The position of the dual-microelectrode tip was controlled by the approach curves at different normalized currents, and the distances between the dual-microelectrode tip and the cells were calculated according to Formula 2 with 12.5 μm in the radius of the microelectrode and 50.0 μm in r_g. When the dual-microelectrode tip was stopped at normalized current values of 0.55, 0.75, 0.85, 0.95, 0.97 and 0.98, the corresponding distances between the dual-microelectrode tip and cell were calculated as 10, 20, 30, 66, 91 and 117 μm respectively, by substituting these parameters into Formula 2. Then, the potential values at different distances and in the bulk solution were measured, and thus the pH values were obtained according to Formula 1.

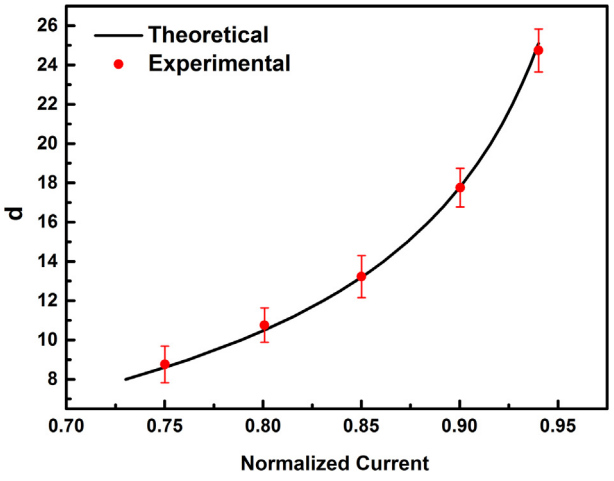

Fig. 2. Theoretical and experimental relationship between the normalized current and the tip-cell distance.

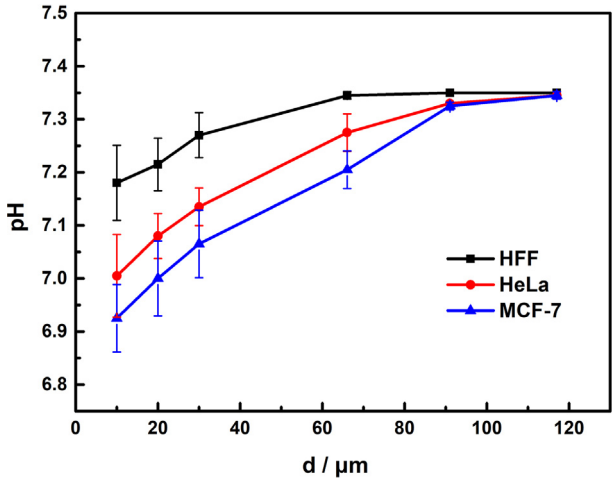

Fig. 3. Measured pH values at different distances in the extracellular space of HFF cells (black line), HeLa cells (red line), and MCF-7 cells (blue line).

Fig. 3 shows the pH values at different distances from HFF, MCF-7, and HeLa cells. Clearly, the pH value near the cell is related to the distance. It increases as the tip moves away from the cells and finally is close to the pH of the solution (7.34), which is contributed by the diffusion of H^+ in the solution. Therefore, the pH measured closer to the cell could reflect the microenvironment of the cell more accurately. Considering that the tip could cause damage to the cell at very close distance, the pH measured at a distance of 20 μm from the cell is referred as pHe. Furthermore, it could be observed that for HFF cells, as the distance increases from 10 μm to 66 μm, the pH increases from 7.18 to 7.34, and the almost constant value was detected at larger distances. In regard to HeLa cells, the pH increases from 7.01 to 7.33 when the distance varies from 10 μm to 91 μm, and then the value shows little change. The pH of MCF-7 cells increases from 6.93 and reaches the plateau of 7.33 at the distance of 91 μm. Obviously, these three cell types present different variation trend of pHe with distance, showing that HeLa and MCF-7 cells have lower pHe values than HFF cells because cancer cells were more acidic [41]. The results suggest that pHe could be a characteristic of cells.

3.4. pHe change of different cell types under electrical stimulation

Different cell types not only have different pHe, but also exhibit different responses on pHe to the changes in the external conditions of cells. To investigate the influence of electrical stimulation on pHe, HFF, MCF-7 and HeLa cells were stimulated at different potentials

Table 2
Measured distances corresponding to different normalized currents.

I_T	0.75	0.80	0.85	0.90	0.94
d (μm)	8.76 ± 0.93	10.76 ± 0.88	13.22 ± 1.07	17.75 ± 0.98	24.74 ± 1.10

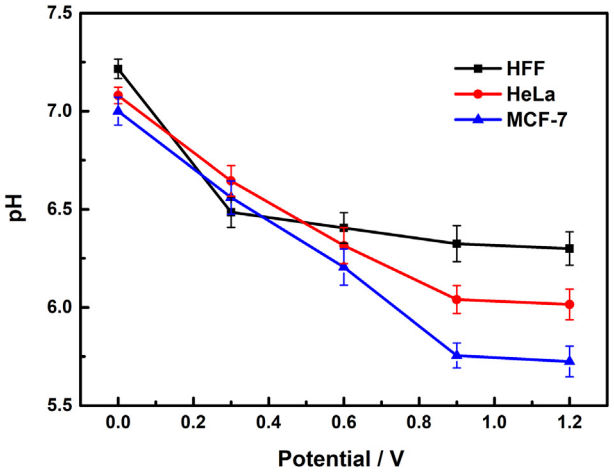

Fig. 4. Measured pHe values in 0.01 M PBS at a distance of 20 μm from the HFF cells (black line), HeLa cells (red line), and MCF-7 cells (blue line) under different stimulation potentials for 60 s.

for 60 s, followed by the potentiometric determination of pHe at a distance of 20 μm from the cell.

As shown in Fig. 4, pHe of HFF cells decreases significantly from 7.22 to 6.49 at a stimulation potential of 0.3 V. While, when the stimulation potential increases from 0.3 to 1.2 V, pHe only changes from 6.49 to 6.30. In regard to HeLa cells, when the stimulation potential increases from 0 to 0.9 V, pHe gradually decreases from 7.08 to 6.04 and remains nearly the same at further increased stimulation potential. For MCF-7 cells, pHe uniformly decreases from 7.00 to 5.76 as the stimulation potential increases from 0 to 0.9 V and the stimulation at a higher potential doesn't cause the further decrease of pHe. Clearly, the pHe of three cell types all decreases under electrical stimulation, which is consistent with the phenomenon reported in the literatures [4,42]. This result might be caused by the increased membrane permeability under electrical stimulation, thus accelerating the release of intracellular acidic material. Nevertheless, different cell types show different response sensitivities to electrical stimulation. In regard to the HeLa and MCF-7 cells, with the increase in stimulation potential, the pHe values of these cancer cells gradually and continuously decrease, probably due to the high amount of intracellular acidic material in tumor cells. When the stimulation potential is higher than 0.9 V, the pHe values of these cancer cells basically do not change. It is possible that the membrane permeability reaches its maximum at this time, or is even destroyed causing cell death. While, the pHe value of HFF cells changes significantly under low-potential stimulation, indicating that they are more sensitive to potential stimulation. However, the value shows little variation under stimulation at high potential. The results indicate that the in situ observation of pHe changes could reveal the response of different cells to different environmental stimuli.

To observe the cell state after electrical stimulation, the cells were fluorescently stained with calcein-AM and propidium iodide [31]. Calcein-AM can pass through the cell membrane, and the AM of calcein-AM is removed by the esterase action of living cells, so the living cells emit a green fluorescence under fluorescence microscopy [4]. At the same time, propidium iodide enters the damaged cell membrane and embeds in the DNA double helix of the cell, thus providing red fluorescence [4]. The damage of cell membrane will not only affect the viability of the cells, but also change the permeability of cell membrane. Therefore, fluorescence staining can roughly verify the changes of cell membrane permeability.

Fig. 5 shows the fluorescence images of MCF-7 cells (a-d), HeLa cells (e-h) and HFF cells (i-l) that were unstimulated and stimulated at 0.3 V, 0.9 V and 1.2 V for 60 s, respectively. It could be observed that without stimulation, all three cell types basically exhibit green fluorescence. In regard to the MCF-7 and HeLa cells, some cells exhibit red fluorescence under 0.3 V of electrical stimulation, and as the potential increases to 0.9 V, the number of cells exhibiting red fluorescence significantly

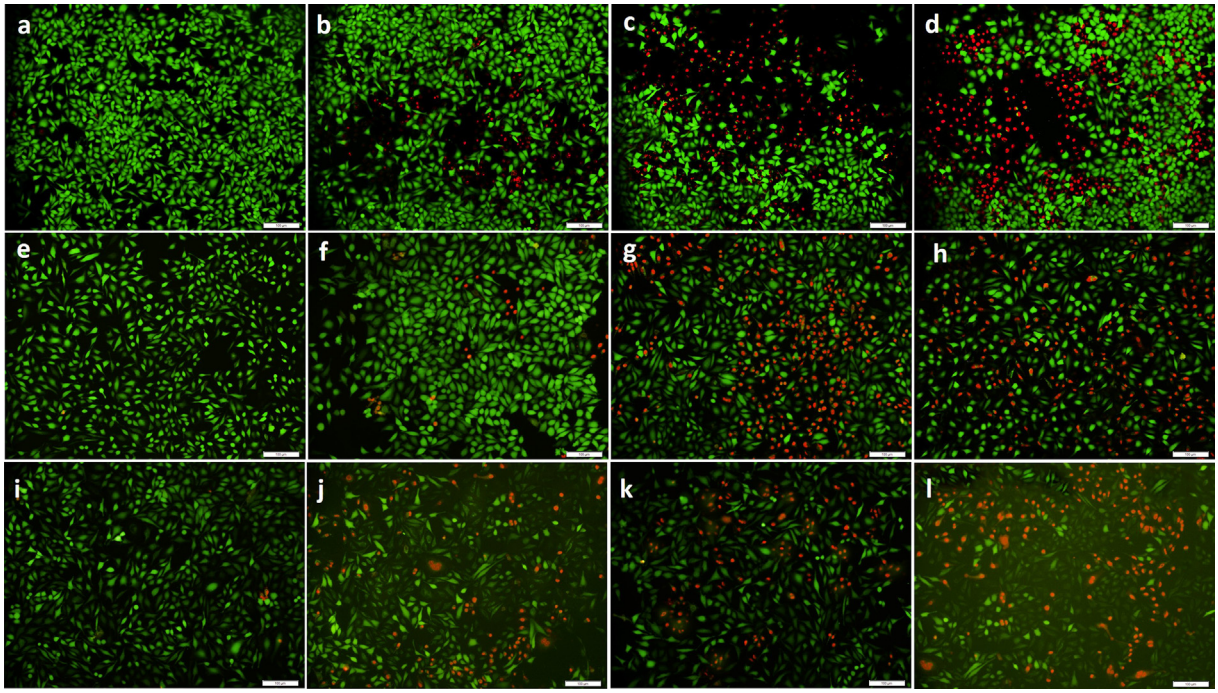

Fig. 5. Calcein-AM/propidium iodide staining of HFF cells, HeLa cells and MCF-7 cells under different stimulation potentials for 60 s. MCF-7 cells: (a) 0 V, (b) 0.3 V, (c) 0.9 V, and (d) 1.2 V; HeLa cells: (e) 0 V, (f) 0.3 V, (g) 0.9 V, and (h) 1.2 V; and HFF cells: (i) 0 V, (j) 0.3 V, (k) 0.9 V, and (l) 1.2 V. The scale bars are 100 μm.

increases. The electrical stimulation at 1.2 V present similar result to that at 0.9 V. For HFF cells, more cells exhibit red fluorescence under 0.3 V of electrical stimulation, and the number of cells that show red fluorescence only slightly increases even when the potential increased to 0.9 and 1.2 V. The results indicate that electrical stimulation could increase the cell membrane permeability, and different cell types have different sensitivities to electrical stimulation. The permeability of cancer cells increases as the stimulation potential increases. When the potential is higher than 0.9 V, the cell membrane permeability might have reached its maximum. While, the permeability of normal cells increases significantly under low-potential stimulation, and further increase in stimulation potential couldn't cause a significant change in the permeability, revealing that the permeability of normal cells reaches a maximum at a much lower stimulation potential. Therefore, observing the influence of external stimulation on the pHe values is helpful to analyze the released species or other responses of cells.

4. Conclusions

In summary, a dual-microelectrode tip, consisting of an Au microelectrode and a pH-selective microelectrode, was used as the tip of a scanning electrochemical microscope to in situ monitor the pHe changes of different cell types under electrical stimulation. The distance between the dual-microelectrode tip and cell was determined by theoretical calculations. The results showed that the pHe of cancer cells was lower than that of normal cells. By comparing the pHe of different cell types under different electrical stimulation, it was found that these cell types exhibited different changes in pHe after electrical stimulation, due to the different degrees of changes in cell membrane permeability, which were confirmed by fluorescent staining. Observing the changes in the pHe values of cells after electrical stimulation is helpful to further explore the cell responses to stimulation and the reasons for the differences. This work provides a new means for the in situ detection of species released by cells exposed to external stimulation.

CRediT authorship contribution statement

Qiang Xiong: Conceptualization, Methodology, Formal analysis, Investigation, Writing - original draft. **Ranran Song:** Investigation, Formal analysis. **Tao Wu:** Methodology, Validation. **Fan Zhang:** Resources, Writing - review & editing. **Pingang He:** Supervision, Writing - review & editing.

Declaration of Competing Interest

The authors declare that they have no known competing financial interests or personal relationships that could have appeared to influence the work reported in this paper.

Acknowledgments

This work was financially supported by the National Natural Science Foundation of China (Grant No. 21575042).

Appendix A. Supplementary data

Supplementary data to this article can be found online at https://doi.org/10.1016/j.jelechem.2021.115169.

References

[1] D. Cialla-May, X.-S. Zheng, K. Weber, J. Popp, Recent progress in surface-enhanced Raman spectroscopy for biological and biomedical applications: from cells to clinics, Chem. Soc. Rev. 46 (2017) 3945–3961.
[2] C. Corbet, O. Feron, Tumour acidosis: from the passenger to the driver's seat, Nat. Rev. Cancer 17 (2017) 577–593.
[3] B.A. Webb, M. Chimenti, M.P. Jacobson, D.L. Barber, Dysregulated PH: a perfect storm for cancer progression, Nat. Rev. Cancer 11 (9) (2011) 671–677.
[4] G. Qi, H. Li, Y. Zhang, C. Li, S. Xu, M. Wang, Y. Jin, Smart plasmonic nanorobot for real-time monitoring cytochrome c release and cell acidification in apoptosis during electrostimulation, Anal. Chem. 91 (2) (2019) 1408–1415.
[5] M. Xu, X. Ma, T. Wei, Z.-X. Lu, B. Ren, In situ imaging of live-cell extracellular pH during cell apoptosis with surface-enhanced Raman spectroscopy, Anal. Chem. 90 (23) (2018) 13922–13928.
[6] P.M. Enriquez-Navas, R.J. Gillies, Measuring pHi and pHe by MRS, Emagres 4 (2007) 643–650.
[7] A. Lardner, The effects of extracellular pH on immune function, J. Leukoc. Biol. 69 (2001) 522–530.
[8] J.L. Carvalho-de-Souza, B.I. Pinto, D.R. Pepperberg, F. Bezanilla, Optocapacitive generation of action potentials by microsecond laser pulses of nanojoule energy, Biophys. J. 114 (2) (2018) 283–288.
[9] F.P. Filice, M.S.M. Li, J.D. Henderson, Z. Ding, Mapping Cd^{2+}-induced membrane permeability changes of single live cells by means of scanning electrochemical microscopy, Anal. Chim. Acta 908 (2016) 85–94.
[10] F.P. Filice, J.D. Henderson, M.S.M. Li, Z. Ding, Correlating live cell viability with membrane permeability disruption induced by trivalent chromium, ACS Omega 4 (1) (2019) 2142–2151.
[11] C. Daniel, C. Bell, C. Burton, S. Harguindey, S.J. Reshkin, C. Rauch, The role of proton dynamics in the development and maintenance of multidrug resistance in cancer, Biochim. Biophys. Acta 1832 (5) (2013) 606–617.
[12] S.K. Parks, J. Chiche, J. Pouyssegur, pH control mechanisms of tumor survival and growth, J. Cell. Physiol. 226 (2) (2011) 299–308.
[13] G. Ke, Z. Zhu, W. Wang, Y. Zou, Z. Guan, S. Jia, H. Zhang, X. Wu, C.J. Yang, A cell-surface-anchored ratiometric fluorescent probe for extracellular pH sensing, ACS Appl. Mater. Interfaces 6 (17) (2014) 15329–15334.
[14] R.M. Kenney, M.W. Boyce, N.A. Whitman, B.P. Kromhout, M.R. Lockett, A pH-sensing optode for mapping spatiotemporal gradients in 3D paper-based cell cultures, Anal. Chem. 90 (3) (2018) 2376–2383.
[15] T. Pan, C. Yang, J. Li, J. Jiang, J. Wen, Z. Wang, K.e. Zhong, Y. Tian, M. Chen, High-throughput extracellular pH monitoring and antibiotics screening by polymeric fluorescent sensor with LCST property, Methods 168 (2019) 51–61.
[16] S. Zeng, D. Liu, C. Li, F. Yu, L. Fan, C. Lei, Y. Huang, Z. Nie, S. Yao, Cell-surface-anchored ratiometric DNA tweezer for real-time monitoring of extracellular and apoplastic pH, Anal. Chem. 90 (22) (2018) 13459–13466.
[17] J. Wang, Y. Geng, Y. Shen, W. Shi, W. Xu, S. Xu, SERS-active fiber tip for intracellular and extracellular pH sensing in living single cells, Sens. Actuators B: Chem. 290 (2019) 527–534.
[18] C. Pan, X. Li, J. Sun, Z. Li, L. Zhang, W. Qian, P. Wang, J. Dong, A multiplexed SERS-active microneedle for simultaneous redox potential and pH measurements in rat joints, ACS Appl. Bio Mater. 2 (5) (2019) 2102–2108.
[19] F. Sun, P. Zhang, T. Bai, D. David Galvan, H.-C. Hung, N. Zhou, S. Jiang, Q. Yu, Functionalized plasmonic nanostructure arrays for direct and accurate mapping extracellular pH of living cells in complex media using SERS, Biosens. Bioelectron. 73 (2015) 202–207.
[20] L. Bi, Y. Wang, Y. Yang, Y. Li, S. Mo, Q. Zheng, L. Chen, Highly sensitive and reproducible SERS sensor for biological pH detection based on a uniform gold nanorod array platform, ACS Appl. Mater. Interfaces 10 (18) (2018) 15381–15387.
[21] T. Sakata, H. Sugimoto, A. Saito, Live monitoring of microenvironmental pH based on extracellular acidosis around cancer cells with cell-coupled gate ion-sensitive field-effect transistor, Anal. Chem. 90 (21) (2018) 12731–12736.
[22] M.-L. García-Martín, G. Hérigault, C. Rémy, R. Farion, P. Ballesteros, J.A. Coles, S. Cerda´n, A. Ziegler, Mapping extracellular pH in rat brain gliomas in vivo by H Magnetic resonance spectroscopic imaging : comparison with maps of metabolites, Cancer Res. 61 (2001) 6524–6531.
[23] P. Provent, M. Benito, B. Hiba, R. Farion, P. López-Larrubia, P. Ballesteros, C. Re´ my, C. Segebarth, S. Cerda´n, J.A. Coles, M.L. Garcı´a-Martı´n, Serial in vivo spectroscopic nuclear magnetic resonance imaging of lactate and extracellular pH in rat gliomas shows redistribution of protons away from sites of glycolysis, Cancer Res. 67 (2007) 7638–7645.
[24] A. Valiūnienė, J. Petronienė, M. Dulkys, A. Ramanavičius, Investigation of active and inactivated yeast cells by scanning electrochemical impedance microscopy, Electroanalysis 32 (2020) 367–374.
[25] J. Petroniene, I. Morkvenaite-Vilkonciene, R. Miksiunas, D. Bironaite, A. Ramanaviciene, L. Mikoliunaite, A. Kisieliute, K. Rucinskas, V. Janusauskas, I. Plikusiene, S. Labeit, A. Ramanavicius, Evaluation of redox activity of human myocardium-derived mesenchymal stem cells by scanning electrochemical microscopy, Electroanalysis 32 (2020) 1337–1345.
[26] J. Petroniene, I. Morkvenaite-Vilkonciene, R. Miksiunas, D. Bironaite, A. Ramanaviciene, K. Rucinskas, V. Janusauskas, A. Ramanavicius, Scanning electrochemical microscopy for the investigation of redox potential of human myocardium-derived mesenchymal stem cells grown at 2D and 3D conditions, Electrohim. Acta 360 (2020) 136956.
[27] I. Morkvenaite-Vilkonciene, A. Ramanaviciene, A. Ramanavicius, 9,10-phenanthrenequinone as a redox mediator for the imaging of yeast cells by scanning electrochemical microscopy, Sens. Actuators B: Chem. 228 (2016) 200–206.
[28] A. Ramanavicius, I. Morkvenaite-Vilkonciene, A. Kisieliute, J. Petroniene, A. Ramanaviciene, Scanning electrochemical microscopy based evaluation of

influence of ph on bioelectrochemical activity of yeast cells - saccharomyces cerevisiae, Colloids Surf. B-Biointerfaces 149 (2017) 1–6.
[29] Vrushali S. Joshi, Partha S. Sheet, Nyssa Cullin, Jens Kreth, Dipankar Koley, Real-time metabolic interactions between two bacterial species using a carbon-based pH microsensor as a scanning electrochemical microscopy probe, Anal. Chem. 89 (20) (2017) 11044–11052.
[30] Raluca-Elena Munteanu, Luciana Stănică, Mihaela Gheorghiu, Szilveszter Gáspár, Measurement of the extracellular pH of adherently growing mammalian cells with high spatial resolution using a voltammetric pH microsensor, Anal. Chem. 90 (11) (2018) 6899–6905.
[31] Ranran Song, Qiang Xiong, Tao Wu, Xin Ning, Fan Zhang, Qingjiang Wang, Pingang He, Real-time monitoring of extracellular pH using a pH-potentiometric sensing SECM dual-microelectrode, Anal. Bioanal. Chem. 412 (15) (2020) 3737–3743.
[32] A. Valiūnienė, T. Sabirovas, J. Petronienė, A. Ramanavičius, Towards the application of fast Fourier transform - scanning electrochemical impedance microscopy (FFT-SEIM), J. Electroanal. Chem. 864 (2020) 114067.
[33] Aušra Valiūnienė, Jurate Petroniene, Inga Morkvenaite-Vilkonciene, Georgi Popkirov, Almira Ramanaviciene, Arunas Ramanavicius, Redox-probe-free scanning electrochemical microscopy combined with fast Fourier transform electrochemical impedance spectroscopy, Phys. Chem. Chem. Phys. 21 (19) (2019) 9831–9836.
[34] Inga Morkvenaite-Vilkonciene, Aušra Valiūnienė, Jurate Petroniene, Arunas Ramanavicius, Hybrid system based on fast Fourier transform electrochemical impedance spectroscopy combined with scanning electrochemical microscopy, Electrochem. Commun. 83 (2017) 110–112.
[35] J. Zhang, L.-B. Kong, B. Wang, Y.-C. Luo, L. Kang, In-situ electrochemical polymerization of multi-walled carbon nanotube/polyaniline composite films for electrochemical supercapacitors, Synth. Met. 159 (2009) 260–266.
[36] R.P. Buck, E. Lindner, Recommendations for nomenclature of ionselective electrodes (IUPAC recommendations 1994). Pure Appl. Chem. 66 (1994) 2527–2536.
[37] A.J. Bard, M.V. Mirkin, Scanning Electrochemical Microscopy, 2nd ed., CRC Press, New York, 2012.
[38] B.B. Katemann, A. Schulte, W. Schuhmann, Constant-distance mode scanning electrochemical microscopy (SECM)–Part I: adaptation of a non-optical shear-force-based positioning mode for SECM tips, Chem. Eur. J. 9 (2003) 2025–2033.
[39] A. Hengstenberg, C. Kranz, W. Schuhmann, Facilitated tip-positioning and applications of non-electrode tips in scanning electrochemical microscopy using a sheer force based constant-distance mode, Chem. Eur. J. 6 (2000) 1547–1554.
[40] C. Kranz, G. Friedbacher, B. Mizaikoff, Integrating an ultramicroelectrode in an AFM cantilever: combined technology for enhanced information, Anal. Chem. 73 (2001) 2491–2500.
[41] Michael Kraus, Bernhard Wolf, Implications of acidic tumor microenvironment for neoplastic growth and cancer treatment: a computer analysis, Tumor Biol. 17 (3) (1996) 133–154.
[42] J.C. Thrash, J.D. Coates, Review: direct and indirect electrical stimulation of microbial metabolism, Environ. Sci. Technol. 11 (2008) 42.